Report

Current Biology

MPS1 localizes to end-on microtubule-attached kinetochores to promote microtubule release

Highlights

- MPS1 transiently binds to end-on microtubule-attached kinetochores
- The balance of Aurora B and PP2A-B56 activities determines MPS1 recruitment
- MPS1 autophosphorylation modulates MPS1 kinetochore level but is subordinate to Aurora B
- At end-on attached kinetochores, localized MPS1 promotes microtubule release

Authors

Daniel Hayward, Emile Roberts, Ulrike Gruneberg

Correspondence

ulrike.gruneberg@path.ox.ac.uk

In brief

Hayward et al. show that the spindle checkpoint kinase MPS1 coordinates error correction of microtubule-kinetochore attachments with spindle checkpoint initiation by transiently localizing to end-on attached kinetochores. MPS1 recruitment is Aurora B dependent and opposed by PP2A-B56 and promotes the removal of incorrect microtubule attachments.

Hayward et al., 2022, Current Biology *32*, 5200–5208
December 5, 2022
https://doi.org/10.1016/j.cub.2022.10.047

CellPress

CellPress
OPEN ACCESS

Current Biology

Report

MPS1 localizes to end-on microtubule-attached kinetochores to promote microtubule release

Daniel Hayward,[1,2,3] Emile Roberts,[1,3] and Ulrike Gruneberg[1,4,*]
[1]Sir William Dunn School of Pathology, University of Oxford, South Parks Road, Oxford, Oxfordshire OX1 3RE, UK
[2]Present address: Randall Centre for Cell and Molecular Biophysics, King's College London, London SE1 1UL, UK
[3]These authors contributed equally
[4]Lead contact
*Correspondence: ulrike.gruneberg@path.ox.ac.uk
https://doi.org/10.1016/j.cub.2022.10.047

SUMMARY

In eukaryotes, the spindle assembly checkpoint protects genome stability in mitosis by preventing chromosome segregation until incorrect microtubule-kinetochore attachment geometries have been eliminated and chromosome biorientation has been completed. These error correction and checkpoint processes are linked by the conserved Aurora B and MPS1 Ser/Thr kinases.[1,2] MPS1-dependent checkpoint signaling is believed to be initiated by kinetochores without end-on microtubule attachments,[3,4] including those generated by Aurora B-mediated error correction. The current model posits that MPS1 competes with microtubules for binding sites at the kinetochore.[3,4] MPS1 is thought to first recognize kinetochores not blocked by microtubules and then initiate checkpoint signaling. However, MPS1 is also required for chromosome biorientation and correction of microtubule-kinetochore attachment errors.[5–9] This latter function, which must require direct interaction with microtubule-attached kinetochores, is not readily explained within the constraints of the current model. Here, we show that MPS1 transiently localizes to end-on attached kinetochores and that this recruitment depends on the relative activities of Aurora B and its counteracting phosphatase PP2A-B56 rather than microtubule-attachment state per se. MPS1 autophosphorylation also regulates MPS1 kinetochore levels but does not determine the response to microtubule attachment. At end-on attached kinetochores, MPS1 actively promotes microtubule release together with Aurora B. Furthermore, in live cells, MPS1 is detected at attached kinetochores before the removal of microtubules. During chromosome alignment, MPS1, therefore, coordinates both the resolution of incorrect microtubule-kinetochore attachments and the initiation of spindle checkpoint signaling.

RESULTS AND DISCUSSION

MPS1 can localize to end-on attached kinetochores

MPS1 has been shown to promote microtubule release when tethered to microtubule-attached kinetochores,[9] but it has so far remained unclear when MPS1 carries out this role physiologically, given that competition with microtubules has been proposed to prevent MPS1 from binding to microtubule-attached kinetochores.[3,4] We assessed an alternative model in which MPS1 recruitment to kinetochores was coupled to microtubule occupancy through kinase and phosphatase activities regulating the state of the kinetochore rather than through direct competition for binding sites alone (Figure 1A). Two lines of evidence support this idea. First, the centromeric Aurora B kinase is known to promote MPS1 kinetochore localization directly, independently from its role in generating microtubule-free, unattached kinetochores.[10–15] Second, the balance between the kinase activity of Aurora B and the opposing phosphatase PP2A-B56, respectively, is critical for MPS1 binding and release at unattached kinetochores.[10] A phosphorylation state change model predicts a transition state in which MPS1 and microtubules are bound to kinetochores simultaneously. First, it was important to ascertain that under physiological conditions, end-on microtubule-attached kinetochores with high levels of MPS1 could be observed. As predicted, in prometaphase cells, kinetochores staining positive for the attached-kinetochore marker Astrin,[16,17] as well as for MPS1, were present in small numbers (Figures S1A–S1D). We hypothesized that if MPS1 localization was controlled by transitions between phosphorylation states then the stability of these states would be temperature-sensitive. To test this, we used an established cold-treatment method, originally aimed at distinguishing stable end-on from transient microtubule-kinetochore attachments.[18] A brief cold treatment significantly increased the number of end-on attached kinetochores exhibiting levels of MPS1 equivalent to unattached kinetochores, at metaphase plates (Figures 1B and 1C). To facilitate the direct comparison of microtubule-attached and unattached states in the same cell, we performed the same analysis in HeLa cells treated with the KIF11/Eg5 inhibitor S-Trityl-L-cysteine (STLC) to create monopolar spindles. Kinetochore pairs in monopolar spindles typically contain one attached and one unattached kinetochore, and cold treatment resulted in an elevated frequency of kinetochores displaying equivalent MPS1 levels on both kinetochores (Figures 1D, 1E, and

CellPress
OPEN ACCESS

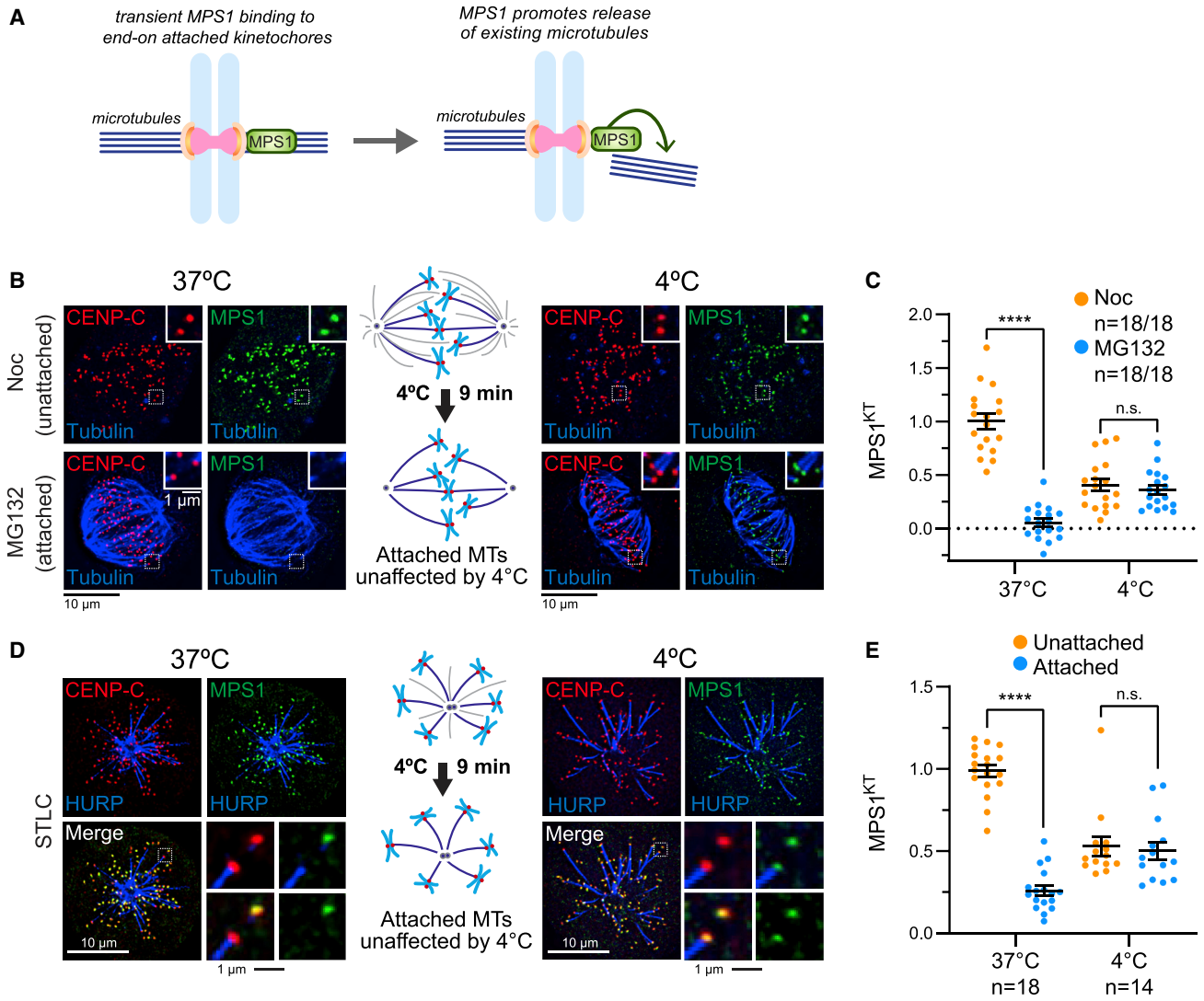

Figure 1. MPS1 can localize to end-on attached kinetochores

(A) Schematic diagram depicting transient MPS1 binding to microtubule-attached kinetochores.

(B) Nocodazole (Noc) or MG132 arrested HeLa MPS1-GFP cells were either directly fixed or cooled to 4°C for 9 min then fixed and immunostained as indicated.

(C) MPS1 kinetochore cell average intensities of cells in (B). Bars show mean ± SEM. ****$p \leq 0.0001$.

(D) STLC-arrested HeLa MPS1-GFP cells treated as in (B). The K-fiber marker HURP was used to visualize kinetochore attachments.[19,20]

(E) MPS1 kinetochore cell average intensities of cells in (D). ****$p \leq 0.0001$.

See also Figure S1.

S1E–S1G). Importantly, the nature and appearance of microtubule-kinetochore attachments and inter-kinetochore distances were not changed under these conditions (Figures S1H–S1L). Together, these data suggest that MPS1 localization is controlled enzymatically rather than by direct competition with microtubules alone.

PP2A-B56 phosphatase activity is required for loss of MPS1 from attached kinetochores

Prompted by our previous observation that the phosphatase PP2A-B56 regulates MPS1 levels at unattached kinetochores by opposing Aurora B,[10] we then asked if the inhibition of specific phosphatase activities would stabilize MPS1 localization to attached kinetochores. To test this idea, we examined endogenous MPS1 localization in HeLa MPS1-GFP cells,[21] briefly treated with the potent PP2A and PP1 inhibitor calyculin A. Compared with control cells, this treatment significantly increased the amount of MPS1 detected at bioriented end-on attached kinetochores at metaphase plates (Figures 2A, 2B, S2A, and S2B). Previous work had established that PP2A-B56 is recruited to kinetochores via association with BUBR1.[22,23] To test the involvement of this specific pool of PP2A-B56, we replaced endogenous BUBR1 with the PP2A-B56 binding deficient BUBR1-L669A/I672A mutant (BUBR1$^{LI/AA}$) (Figure S2G).[22,24] The replacement of BUBR1 with mCherry-BUBR1$^{LI/AA}$ in STLC-treated monopolar spindles reduced the number of

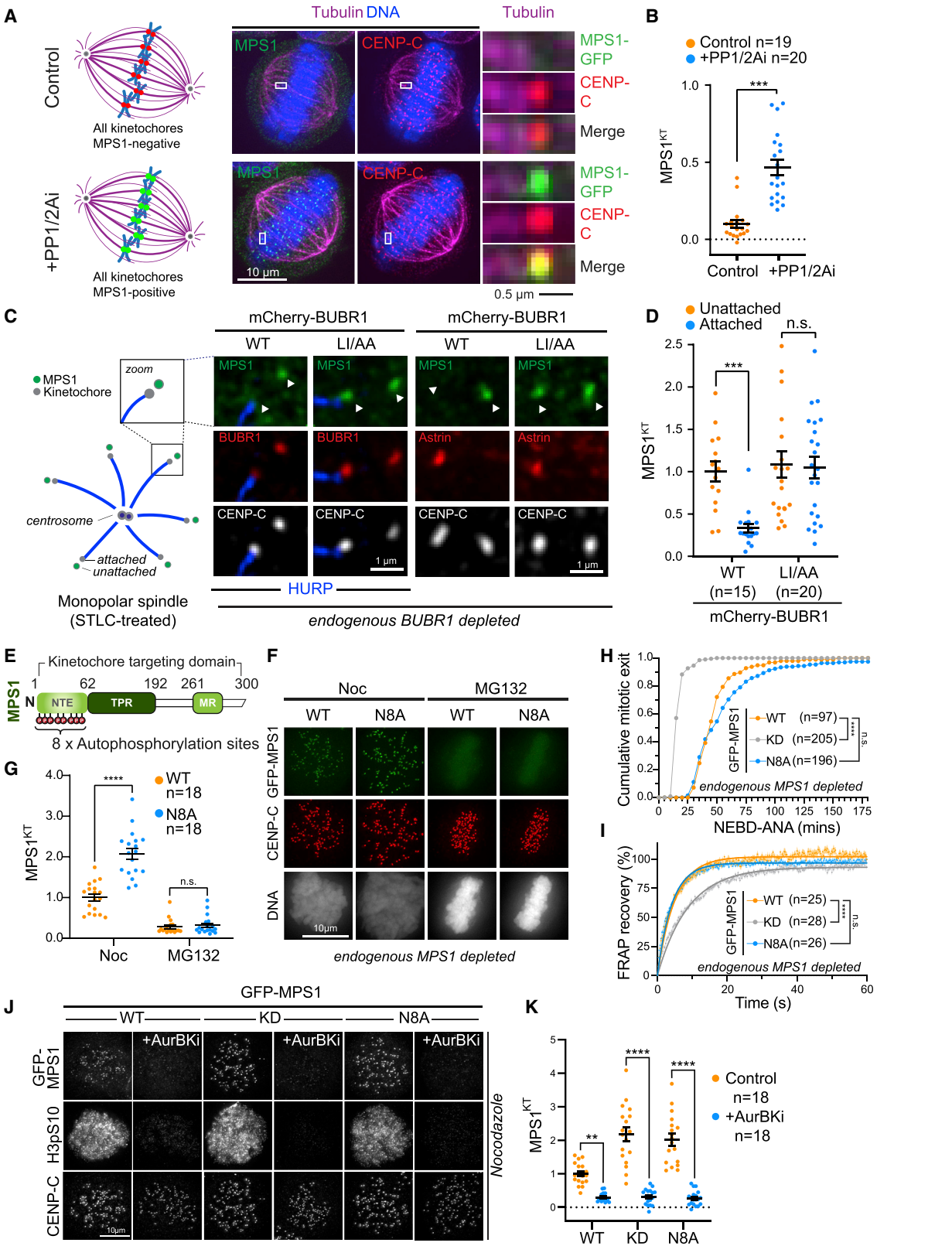

(legend on next page)

microtubule-attached kinetochores (Figures S2H–S2J), but in kinetochore pairs with a clear end-on attachment, MPS1 was recruited to both the attached and the unattached kinetochore at equivalent levels, as also observed for calyculin A treatment (Figures 2C, 2D, and S2C–S2F). These observations demonstrate that kinetochore-bound PP2A-B56 is required for kinetochores to transition into a state in which MPS1 will not localize. Presumably, this relationship underpins the transition state we observed under physiological conditions (Figures S1A–S1D). We set out to understand how the kinase activities of MPS1 and Aurora B influence these state transitions.

N-terminal autophosphorylation controls the MPS1 steady-state kinetochore level but not a response to attachment

Autophosphorylation of the N-terminal kinetochore-binding domain of MPS1 has been shown to modulate its localization at unattached kinetochores.[25,26] To test the importance of this mechanism, we generated GFP-tagged MPS1 mutants lacking all known autophosphorylation sites at S7, T12, T33, and S37[25] and S15, T45, T46, and S49[27] (Figure 2E) and used this version of MPS1, GFP-MPS1^{N8A}, to replace the endogenous protein (Figure S2K). GFP-MPS1^{N8A} accumulated to 2–2.5 times higher levels than GFP-MPS1^{WT} at unattached kinetochores (Figures 2F, 2G, S2L, and S2M), similarly to kinase-dead MPS1 (GFP-MPS1^{KD}).[6,28] Importantly, GFP-MPS1^{N8A} recruitment to kinetochores was not increased further by MPS1 inhibition,[6] suggesting that all relevant autophosphorylation sites had been mutated (Figures S2L and S2M). Corroborating these findings, phospho-mimetic mutations of the same sites (GFP-MPS1^{N8E}) resulted in poor kinetochore localization, which was not increased upon MPS1 inhibition (Figures S2L and S2M). If autophosphorylation of the MPS1 N terminus was the key reason for the loss of MPS1 from attached kinetochores, GFP-MPS1^{N8A} should remain localized to attached kinetochores in metaphase cells. However, like GFP-MPS1^{WT}, GFP-MPS1^{N8A} was not observed on attached kinetochores at metaphase plates or in a monopolar spindle situation (Figures 2F, 2G, S2N, and S2O) and behaved very similarly to GFP-MPS1^{WT}, but differently from GFP-MPS1^{KD},[28] in fluorescence recovery after photobleaching (FRAP) ($t_{1/2}$ 3.7 ± 1.3 s for WT; 2.9 ± 0.9 s for N8A; 6.4 ± 2.1 s for KD) and live cell imaging experiments (Figures 2H and 2I). This suggests that the removal of MPS1 from kinetochores is not affected by the absence of the N-terminal autophosphorylation sites. Therefore, we conclude that, although MPS1 N-terminal autophosphorylation does modulate the levels of MPS1 at unattached kinetochores, it is not the mechanism conferring sensitivity to microtubule attachment. Interestingly, kinase-dead GFP-MPS1^{KD}, in contrast to GFP-MPS1^{N8A}, showed some localization to attached kinetochores (Figures S2N and S2O). This difference is due to the fact that kinase-dead or inhibited MPS1 cannot recruit BUBR1 and associated PP2A-B56,[22,23] which normally opposes Aurora B-dependent MPS1 recruitment[10] (Figures S2P–S2S). Hence, for inactive MPS1, localization to attached kinetochores in monopolar spindles (Figures S2N and S2O) or at metaphase plates is observed (Figures S2T and S2U). This is similar to what is seen upon PP2A inhibition (Figures 2A and 2B) or loss of kinetochore B56 (Figures 2C and 2D), further confirming the importance of PP2A-B56 for correct MPS1 localization.

Aurora B-dependent localization of MPS1 to kinetochores can be uncoupled from the microtubule-attachment status

We next explored the role of Aurora B activity in MPS1 recruitment to kinetochores. The inhibition of Aurora B[29] results in the loss of MPS1 from unattached kinetochores, including the MPS1^{KD} (kinase-dead) and MPS1^{N8A} mutants that cannot be auto-phosphorylated[6,10,13] (Figures 2J and 2K). To test whether Aurora B activity at kinetochores is not only necessary but also sufficient for MPS1 recruitment, we created a situation where Aurora B activity could be modulated at microtubule-attached kinetochores. For this, we generated HeLa cells expressing both endogenously GFP-tagged MPS1 and a rapamycin-dependent dimerization module that recruits a truncated version of the Aurora B interaction partner INCENP, together with Aurora B, to the outer kinetochore protein Mis12 upon rapamycin addition[15,30] (Figure 3A). These cells were then arrested at metaphase, so all kinetochores were fully attached (Figure 3B, middle; Figure 3D, −1 min). Upon rapamycin addition active, T232-phosphorylated, Aurora B accumulated at kinetochores to levels similar to those found on prometaphase centromeres (Figures 3B and 3C). Live cell imaging showed that this

Figure 2. PP2A-B56 phosphatase activity is required for the loss of MPS1 from attached kinetochores

(A) HeLa MPS1-GFP cells arrested with MG132 and treated with calyculin A (PP1/2Ai) were immunostained as indicated. Blow-ups of representative attached kinetochores are on the right.

(B) Cell averages of kinetochore-MPS1 intensities at attached metaphase kinetochores in cells in (A). Scale bars represent mean ± SEM. Values were normalized to the levels of MPS1 at unattached kinetochores without PP1/2Ai treatment (Figures S2A and S2B). ***p ≤ 0.001.

(C) STLC-arrested HeLa Flp-In TREx GFP-MPS1 cells depleted of endogenous BUBR1 and expressing mCherry-BUBR1^{WT} or mCherry-BUBR1$^{LI/AA}$ were immunostained as indicated. Arrowheads indicate kinetochore positions.

(D) Cell averages of kinetochore-MPS1 in cells in (C). Bars show mean ± SEM. ***p ≤ 0.001.

(E) Schematic diagram of the MPS1 N-terminal kinetochore targeting domain and autophosphorylation sites.

(F) HeLa Flp-In TREx cells depleted of endogenous MPS1 and expressing GFP-MPS1 transgenes treated with nocodazole and MG132 (Noc) or MG132 alone were fixed and stained as indicated.

(G) Cell averages of MPS1 kinetochore intensities of cells in (F). Bars indicate mean ± SEM. ****p ≤ 0.0001.

(H) Plot of cumulative mitotic exit of HeLa Flp-In TREx cells depleted of endogenous MPS1 and expressing GFP-MPS1 transgenes. ****p ≤ 0.0001.

(I) Average fluorescence recovery after photobleaching curves from nocodazole-arrested HeLa Flp-In TREx cells depleted of endogenous MPS1 and expressing GFP-MPS1 transgenes. ****p ≤ 0.0001.

(J) HeLa Flp-In TREx cells depleted of endogenous MPS1 and expressing GFP-MPS1 transgenes arrested with nocodazole and MG132 were treated with AurBKi for 10 min and immunostained as indicated.

(K) Cell averages of MPS1 kinetochore intensity from cells in (J). Bars show mean ± SEM. ****p ≤ 0.0001.

See also Figure S2.

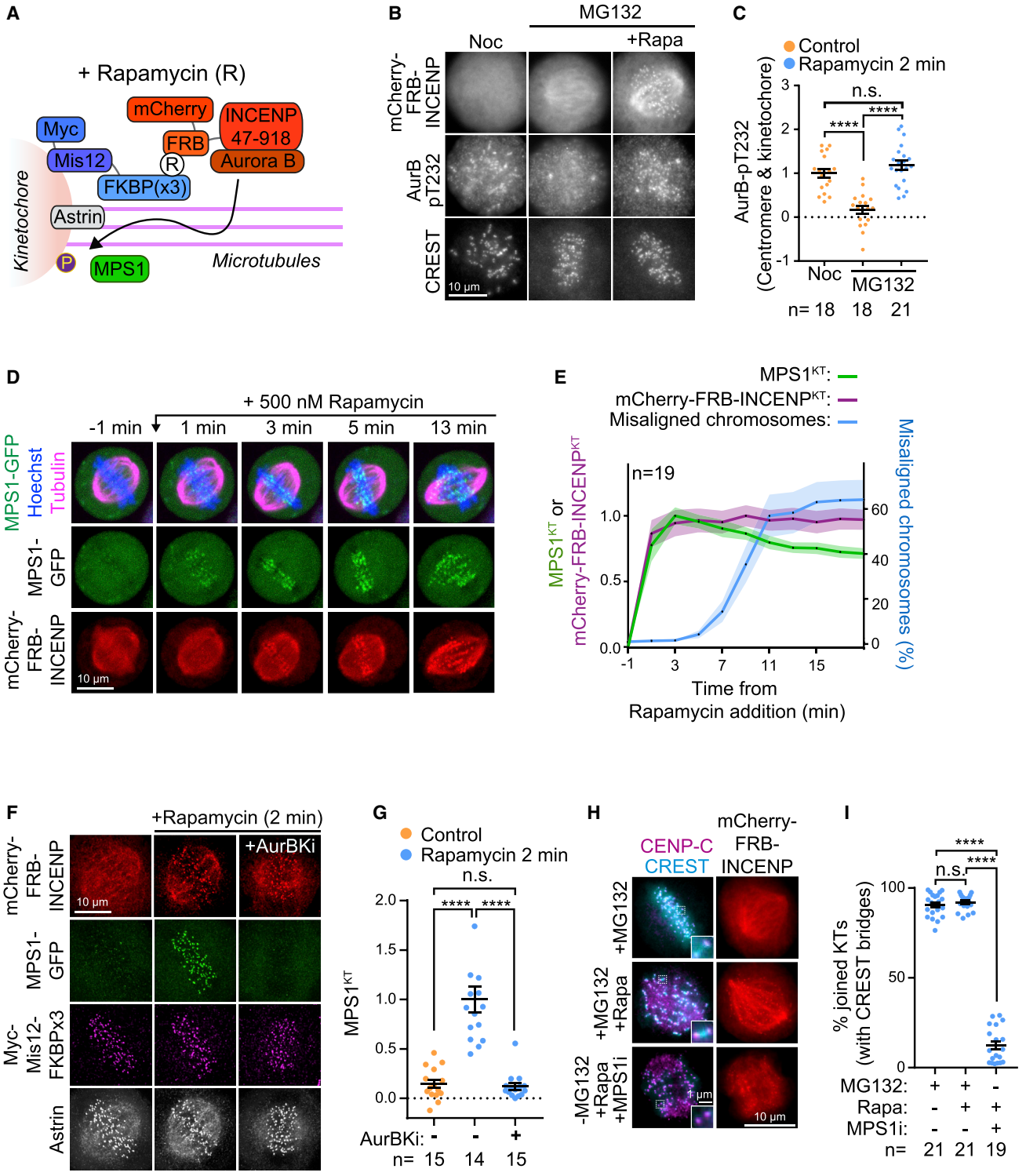

Figure 3. Aurora B-dependent localization of MPS1 to kinetochores can be uncoupled from the microtubule-attachment status

(A) Diagram of the rapamycin-dependent dimerization module used to recruit INCENP-Aurora B to the kinetochore protein Mis12.

(B) HeLa MPS1-GFP cells expressing the Aurora B kinetochore targeting system were arrested with nocodazole or MG132 , then treated with rapamycin for 2 min as indicated and stained for Aurora B-pT232.

(C) Plot of Aurora B-pT232 centromere and kinetochore intensities. Bars represent mean ± SEM. ****p ≤ 0.0001.

(D) Movie stills of HeLa MPS1-GFP cells expressing the Aurora B kinetochore targeting system treated with MG132. Cell at −1 min is at metaphase prior to the addition of rapamycin. Tubulin and DNA were visualized with SiR-Tubulin and Hoechst.

(legend continued on next page)

specifically resulted in the rapid recruitment of endogenous MPS1-GFP to end-on attached kinetochores, to levels comparable with those at unattached kinetochores (Figures 3D, 3E, S3A, and S3B). As a consequence of this, downstream spindle checkpoint proteins such as MAD1, BUB1, and BUBR1 were now also detected on these kinetochores (Figures S3C–S3G). This MPS1 recruitment to attached kinetochores was completely dependent on Aurora B activity (Figures 3F and 3G). Interestingly, cold-stable microtubule attachment was maintained on average for 4–5 min after rapamycin addition but then started to resolve, leading to chromosomes leaving the metaphase plate (Figures 3D, 3E, and S3H–S3J). Although the loss of one-sided microtubule-kinetochore attachment resulted in anaphase-like chromosome movements, sister chromatid cohesion was maintained (Figures 3H and 3I). In summary, these data demonstrate that MPS1 can be recruited to microtubule-attached kinetochores as long as Aurora B activity exceeds a threshold level. When kinetochores bi-orient, Aurora B activity is attenuated through spatial separation from its substrates,[15] and PP2A-B56 activity triggers the loss of MPS1[10] (Figures 2C and 2D). HEC1/NDC80 is the key microtubule-binding component of the outer kinetochore and has been suggested to constitute the crucial Aurora B regulated binding site for MPS1 at unattached kinetochores.[4,31] However, although HEC1/NDC80 presence is required for MPS1 recruitment,[12,13] mutations of all described Aurora phosphorylation sites in HEC1/NDC80[32] to alanine or phospho-mimetic aspartate did not reduce MPS1 recruitment or render it resistant to Aurora B inhibition, confirming previous reports[12] (Figures S3K, S3O, and S3P), and did not change MPS1 behavior in response to microtubule attachment (Figures S3L–S3N). NDC80 itself is thus unlikely to be the crucial target of Aurora B for promoting the recruitment of MPS1.

At end-on attached kinetochores, localized MPS1 promotes microtubule release

MPS1 has been described as an important factor for error correction,[5–9] yet when this activity occurs and how it is coordinated with Aurora B has not been elucidated. Our findings suggest that transient MPS1 localization to end-on attached kinetochores is important. To investigate this, we repeated the rapamycin-induced Aurora B recruitment to kinetochores in the presence of an MPS1 inhibitor. This did not alter the subsequent recruitment of endogenous MPS1 to attached kinetochores (Figure 4A). However, MPS1 inhibition resulted in a marked delay in the loss of kinetochore attachments in comparison with control cells (Figures 4A, 4B, and S3J), consistent with an important contribution by MPS1 to the prompt resolution of incorrect attachments, as previously observed for kinetochore-tethered MPS1.[9] To confirm MPS1 functionality in a physiological setting, high-resolution imaging of MPS1 at syntelic attachments undergoing error correction was carried out. This showed that endogenous MPS1 localization to end-on attached kinetochores precedes the loss of attachment (Figures 4C and 4D), confirming the idea that the transient presence of MPS1 at end-on attached kinetochores is required for the timely removal of the attachment. In summary, our findings suggest that MPS1 is recruited to kinetochores marked by high Aurora B phosphorylation (Figure 4Ei). If the attachment stabilizes and Aurora B is attenuated, then MPS1 leaves the kinetochore (Figure 4Eii); otherwise, MPS1 then helps destabilize the attachment and create an unattached kinetochore while simultaneously promoting the recruitment of the components of the spindle assembly checkpoint machinery (Figure 4Eiii). By recruiting BUBR1, MPS1 also indirectly promotes the kinetochore localization of the phosphatase PP2A-B56 that is needed to ultimately stabilize microtubule attachments[9,22,23,33] but also controls MPS1 binding to kinetochores (Figures 2A–2D). This arrangement constitutes an incoherent feedforward loop in which MPS1 concurrently controls the removal as well as the stabilization of kinetochore microtubules (Figure 4F). Using an established assay,[9,33] we compared the effects of inhibiting Aurora B or MPS1 on the formation of cold-stable microtubule-kinetochore attachments and bipolar spindle formation when PP2A-B56 was depleted. The inhibition of Aurora B as evidenced by the loss of histone H3-Ser10 phosphorylation (Figures S4A and S4B) or MPS1 both re-established the cold stability of kinetochore fibers to a similar extent (Figures 4G and 4H). However, MPS1 inhibition "rescued" the effect of PP2A-B56 depletion on bipolar microtubule-kinetochore attachments required for an organized spindle morphology more effectively than Aurora B inhibition, suggesting a more direct role for MPS1 on error correction (Figure 4I), consistent with this idea.

Current thinking is influenced by the notion that the Aurora B phosphorylation of NDC80 at incorrect low-tension attachments leads to microtubule detachment and attraction of MPS1 to microtubule-free kinetochores, initiating spindle checkpoint signaling.[2] Here, we demonstrate that during error correction, MPS1 is transiently recruited to end-on attached kinetochores. This pool of MPS1 then contributes to prompt microtubule release and simultaneous checkpoint protein recruitment. Reported MPS1 substrates during this process include SKA3 and HEC1/NDC80.[9,34] It remains unclear how microtubule binding elicits changes in the balance between Aurora B and PP2A-B56 to control MPS1 localization, especially given that HEC1 does not seem to be the functionally relevant target of Aurora B[12] (Figures S3K–S3P). Elucidating this detail is an important future goal that will fully explain how kinetochores are able to sense microtubule attachment. Since the error correction process and the spindle assembly checkpoint are crucial control mechanisms that safeguard genome stability during chromosome segregation, these insights have important implications for cancer research, where inhibitors of both Aurora B and MPS1 are currently in clinical trial.

(E) Quantification of kinetochore intensities of MPS1-GFP (green), mCherry-FRB-INCENP (magenta), or misaligned chromosomes (blue) in cells as shown in (D). The line shows the mean, the shaded areas are SEM.
(F) HeLa cells as in (D) were stained with anti-Myc and anti-Astrin. AurKBi was added for 10 min prior to fixation, and rapamycin at 2 min prior to fixation.
(G) Kinetochore MPS1 cell intensities, normalized to Myc-Mis12 intensities, of cells in (F). Scale bars represent mean ± SEM. ****$p \leq 0.0001$.
(H) HeLa cells as in (D) were either treated with MG132 alone, MG132 and rapamycin, or rapamycin and MPS1i and stained as indicated.
(I) Percentage of joined sister-kinetochores, as visualized by CREST bridges. Bars represent mean ± SEM.
See also Figure S3.

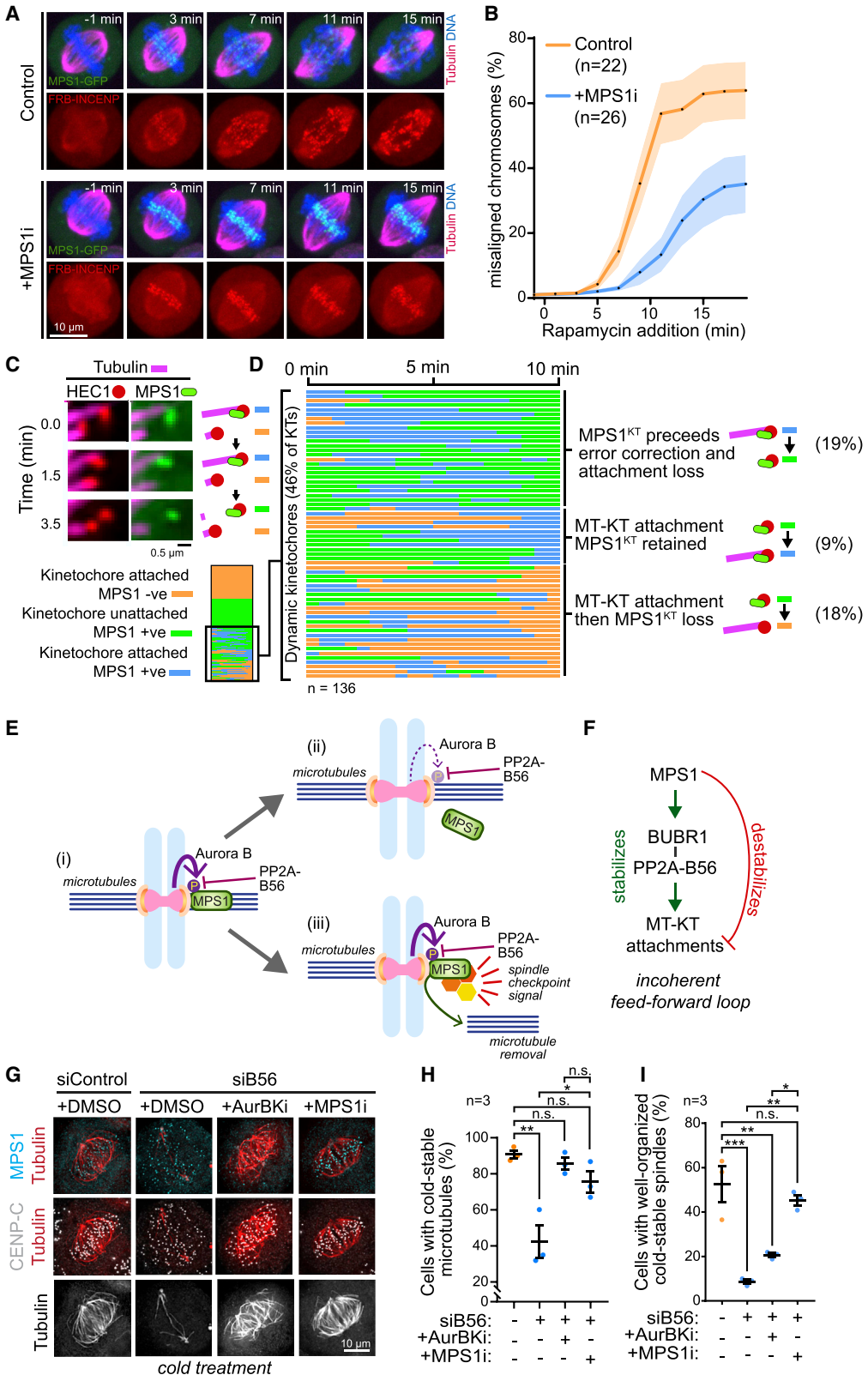

(legend on next page)

STAR★METHODS

Detailed methods are provided in the online version of this paper and include the following:

- KEY RESOURCES TABLE
- RESOURCE AVAILABILITY
  - Lead contact
  - Materials availability
  - Data and code availability
- EXPERIMENTAL MODEL AND SUBJECT DETAILS
  - Cell lines
  - Bacterial strains
- METHOD DETAILS
  - Molecular biology
  - Cell line generation
  - RNAi and RNAi rescue assays
  - Drug and cold treatments
  - Immunofluorescence staining
  - Immunofluorescence microscopy
  - Super-resolution immunofluorescence microscopy
  - Live cell imaging
- QUANTIFICATION AND STATISTICAL ANALYSIS
  - Image processing and analysis
  - Statistical Analysis

SUPPLEMENTAL INFORMATION

Supplemental information can be found online at https://doi.org/10.1016/j.cub.2022.10.047.

ACKNOWLEDGMENTS

We thank Francis Barr for encouragement, advice, and discussions and Bela Novak and Tomoaki Sobajima for their helpful comments on the manuscript. This work was funded by a Cancer Research UK Discovery Programme grant DRCNPG-Nov21\100004 to U.G., a Medical Research Council grant MR/K006703/1 to U.G., an Edward Penley Abraham grant RF 280 to U.G., and a Medical Research Council studentship to E.R. The authors acknowledge that this work would not have been possible without the HeLa cell line, which was developed from Henrietta Lacks' cells taken without compensation or informed consent.

AUTHOR CONTRIBUTIONS

Conceptualization, U.G., D.H., and E.R.; methodology, U.G., D.H., and E.R.; investigation, D.H. and E.R.; visualization, U.G., D.H., and E.R.; funding acquisition, U.G.; project administration, U.G.; supervision, U.G.; writing – original draft, D.H. and U.G.; writing – review & editing, U.G., D.H., and E.R.

DECLARATION OF INTERESTS

The authors declare no competing interests.

Received: May 25, 2022
Revised: September 7, 2022
Accepted: October 20, 2022
Published: November 16, 2022

REFERENCES

1. Musacchio, A. (2015). The molecular biology of spindle assembly checkpoint signaling dynamics. Curr. Biol. *25*, R1002–R1018. https://doi.org/10.1016/j.cub.2015.08.051.
2. Krenn, V., and Musacchio, A. (2015). The Aurora B kinase in chromosome bi-orientation and spindle checkpoint signaling. Front. Oncol. *5*, 225. https://doi.org/10.3389/fonc.2015.00225.
3. Hiruma, Y., Sacristan, C., Pachis, S.T., Adamopoulos, A., Kuijt, T., Ubbink, M., von Castelmur, E., Perrakis, A., and Kops, G.J. (2015). Competition between MPS1 and microtubules at kinetochores regulates spindle checkpoint signaling. Science *348*, 1264–1267. https://doi.org/10.1126/science.aaa4055.
4. Ji, Z., Gao, H., and Yu, H. (2015). Kinetochore attachment sensed by competitive Mps1 and microtubule binding to Ndc80C. Science *348*, 1260–1264. https://doi.org/10.1126/science.aaa4029.
5. Santaguida, S., Tighe, A., D'Alise, A.M., Taylor, S.S., and Musacchio, A. (2010). Dissecting the role of MPS1 in chromosome biorientation and the spindle checkpoint through the small molecule inhibitor reversine. J. Cell Biol. *190*, 73–87. https://doi.org/10.1083/jcb.201001036.
6. Hewitt, L., Tighe, A., Santaguida, S., White, A.M., Jones, C.D., Musacchio, A., Green, S., and Taylor, S.S. (2010). Sustained Mps1 activity is required in mitosis to recruit O-Mad2 to the Mad1-C-Mad2 core complex. J. Cell Biol. *190*, 25–34. https://doi.org/10.1083/jcb.201002133.
7. Maure, J.F., Kitamura, E., and Tanaka, T.U. (2007). Mps1 kinase promotes sister-kinetochore bi-orientation by a tension-dependent mechanism. Curr. Biol. *17*, 2175–2182. https://doi.org/10.1016/j.cub.2007.11.032.
8. Jelluma, N., Brenkman, A.B., van den Broek, N.J., Cruijsen, C.W., van Osch, M.H., Lens, S.M., Medema, R.H., and Kops, G.J. (2008). Mps1 phosphorylates Borealin to control Aurora B activity and chromosome alignment. Cell *132*, 233–246. https://doi.org/10.1016/j.cell.2007.11.046.
9. Maciejowski, J., Drechsler, H., Grundner-Culemann, K., Ballister, E.R., Rodriguez-Rodriguez, J.A., Rodriguez-Bravo, V., Jones, M.J.K., Foley, E., Lampson, M.A., Daub, H., et al. (2017). Mps1 regulates kinetochore-microtubule attachment stability via the ska complex to ensure error-free chromosome segregation. Dev. Cell *41*, 143–156.e6. https://doi.org/10.1016/j.devcel.2017.03.025.
10. Hayward, D., Bancroft, J., Mangat, D., Alfonso-Pérez, T., Dugdale, S., McCarthy, J., Barr, F.A., and Gruneberg, U. (2019). Checkpoint signaling and error correction require regulation of the MPS1 T-loop by PP2A-B56. J. Cell Biol. *218*, 3188–3199. https://doi.org/10.1083/jcb.201905026.

Figure 4. At end-on attached kinetochores, localized MPS1 promotes microtubule release

(A) Movie stills of HeLa MPS1-GFP cells with the Aurora B kinetochore targeting system, arrested with MG132 and treated with or without MPS1i for 10 min prior to imaging. Cells at −1 min are at metaphase before the addition of rapamycin. Tubulin and DNA were visualized with SiR-Tubulin and Hoechst.
(B) Quantification of misaligned chromosomes in cells in (A).
(C) Live cell imaging stills of HeLa MPS1-GFP cells expressing HEC1-mCherry, incubated with SiR-Tubulin and STLC prior to imaging. Shown is an example of an initially syntelically attached-kinetochore pair, where MPS1-GFP localization precedes error correction and attachment loss at one kinetochore.
(D) 136 kinetochores from cells in (C) were assessed for kinetochore attachment status and presence or absence of MPS1-GFP over a 10-min period.
(E) Model for MPS1 recruitment and function (see text for details).
(F) Incoherent feedforward loop describing MPS1 and PP2A-B56 kinetochore recruitment and effector function.
(G) Immunofluorescence analysis of control or PP2A-B56 depleted HeLa MPS1-GFP cells treated with kinase inhibitors before cold treatment.
(H) Quantitation of microtubule stability in cells in (E). *$p \leq 0.05$, **$p \leq 0.01$.
(I) Quantitation of cells with well-organized bipolar spindles in (E). Bars show mean ± SEM. *$p \leq 0.05$, **$p \leq 0.01$, ***$p \leq 0.001$.
See also Figure S4.

11. Santaguida, S., Vernieri, C., Villa, F., Ciliberto, A., and Musacchio, A. (2011). Evidence that Aurora B is implicated in spindle checkpoint signalling independently of error correction. EMBO J. *30*, 1508–1519. https://doi.org/10.1038/emboj.2011.70.

12. Nijenhuis, W., von Castelmur, E., Littler, D., De Marco, V., Tromer, E., Vleugel, M., van Osch, M.H., Snel, B., Perrakis, A., and Kops, G.J. (2013). A TPR domain-containing N-terminal module of MPS1 is required for its kinetochore localization by Aurora B. J. Cell Biol. *201*, 217–231. https://doi.org/10.1083/jcb.201210033.

13. Saurin, A.T., van der Waal, M.S., Medema, R.H., Lens, S.M., and Kops, G.J. (2011). Aurora B potentiates Mps1 activation to ensure rapid checkpoint establishment at the onset of mitosis. Nat. Commun. *2*, 316. https://doi.org/10.1038/ncomms1319.

14. Pinsky, B.A., Kung, C., Shokat, K.M., and Biggins, S. (2006). The Ipl1-Aurora protein kinase activates the spindle checkpoint by creating unattached kinetochores. Nat. Cell Biol. *8*, 78–83. https://doi.org/10.1038/ncb1341.

15. Liu, D., Vader, G., Vromans, M.J., Lampson, M.A., and Lens, S.M. (2009). Sensing chromosome bi-orientation by spatial separation of aurora B kinase from kinetochore substrates. Science *323*, 1350–1353. https://doi.org/10.1126/science.1167000.

16. Schmidt, J.C., Kiyomitsu, T., Hori, T., Backer, C.B., Fukagawa, T., and Cheeseman, I.M. (2010). Aurora B kinase controls the targeting of the Astrin-SKAP complex to bioriented kinetochores. J. Cell Biol. *191*, 269–280. https://doi.org/10.1083/jcb.201006129.

17. Thein, K.H., Kleylein-Sohn, J., Nigg, E.A., and Gruneberg, U. (2007). Astrin is required for the maintenance of sister chromatid cohesion and centrosome integrity. J. Cell Biol. *178*, 345–354. https://doi.org/10.1083/jcb.200701163.

18. Rieder, C.L. (1981). The structure of the cold-stable kinetochore fiber in metaphase PtK1 cells. Chromosoma *84*, 145–158. https://doi.org/10.1007/BF00293368.

19. Dunsch, A.K., Hammond, D., Lloyd, J., Schermelleh, L., Gruneberg, U., and Barr, F.A. (2012). Dynein light chain 1 and a spindle-associated adaptor promote dynein asymmetry and spindle orientation. J. Cell Biol. *198*, 1039–1054. https://doi.org/10.1083/jcb.201202112.

20. Silljé, H.H., Nagel, S., Körner, R., and Nigg, E.A. (2006). HURP is a Ran-importin beta-regulated protein that stabilizes kinetochore microtubules in the vicinity of chromosomes. Curr. Biol. *16*, 731–742. https://doi.org/10.1016/j.cub.2006.02.070.

21. Hayward, D., Alfonso-Pérez, T., Cundell, M.J., Hopkins, M., Holder, J., Bancroft, J., Hutter, L.H., Novak, B., Barr, F.A., and Gruneberg, U. (2019). CDK1-CCNB1 creates a spindle checkpoint-permissive state by enabling MPS1 kinetochore localization. J. Cell Biol. *218*, 1182–1199. https://doi.org/10.1083/jcb.201808014.

22. Kruse, T., Zhang, G., Larsen, M.S., Lischetti, T., Streicher, W., Kragh Nielsen, T., Bjørn, S.P., and Nilsson, J. (2013). Direct binding between BubR1 and B56-PP2A phosphatase complexes regulate mitotic progression. J. Cell Sci. *126*, 1086–1092. https://doi.org/10.1242/jcs.122481.

23. Suijkerbuijk, S.J., Vleugel, M., Teixeira, A., and Kops, G.J. (2012). Integration of kinase and phosphatase activities by BUBR1 ensures formation of stable kinetochore-microtubule attachments. Dev. Cell *23*, 745–755. https://doi.org/10.1016/j.devcel.2012.09.005.

24. Espert, A., Uluocak, P., Bastos, R.N., Mangat, D., Graab, P., and Gruneberg, U. (2014). PP2A-B56 opposes Mps1 phosphorylation of Knl1 and thereby promotes spindle assembly checkpoint silencing. J. Cell Biol. *206*, 833–842. https://doi.org/10.1083/jcb.201406109.

25. Wang, X., Yu, H., Xu, L., Zhu, T., Zheng, F., Fu, C., Wang, Z., and Dou, Z. (2014). Dynamic autophosphorylation of mps1 kinase is required for faithful mitotic progression. PLoS One *9*, e104723. https://doi.org/10.1371/journal.pone.0104723.

26. Koch, L.B., Opoku, K.N., Deng, Y., Barber, A., Littleton, A.J., London, N., Biggins, S., and Asbury, C.L. (2019). Autophosphorylation is sufficient to release Mps1 kinase from native kinetochores. Proc. Natl. Acad. Sci. USA *116*, 17355–17360. https://doi.org/10.1073/pnas.1901653116.

27. Dou, Z., von Schubert, C., Körner, R., Santamaria, A., Elowe, S., and Nigg, E.A. (2011). Quantitative mass spectrometry analysis reveals similar substrate consensus motif for human Mps1 kinase and Plk1. PLoS One *6*, e18793. https://doi.org/10.1371/journal.pone.0018793.

28. Jelluma, N., Dansen, T.B., Sliedrecht, T., Kwiatkowski, N.P., and Kops, G.J. (2010). Release of Mps1 from kinetochores is crucial for timely anaphase onset. J. Cell Biol. *191*, 281–290. https://doi.org/10.1083/jcb.201003038.

29. Ditchfield, C., Johnson, V.L., Tighe, A., Ellston, R., Haworth, C., Johnson, T., Mortlock, A., Keen, N., and Taylor, S.S. (2003). Aurora B couples chromosome alignment with anaphase by targeting BubR1, Mad2, and Cenp-E to kinetochores. J. Cell Biol. *161*, 267–280. https://doi.org/10.1083/jcb.200208091.

30. Ballister, E.R., Riegman, M., and Lampson, M.A. (2014). Recruitment of Mad1 to metaphase kinetochores is sufficient to reactivate the mitotic checkpoint. J. Cell Biol. *204*, 901–908. https://doi.org/10.1083/jcb.201311113.

31. Zhu, T., Dou, Z., Qin, B., Jin, C., Wang, X., Xu, L., Wang, Z., Zhu, L., Liu, F., Gao, X., et al. (2013). Phosphorylation of microtubule-binding protein Hec1 by mitotic kinase Aurora B specifies spindle checkpoint kinase Mps1 signaling at the kinetochore. J. Biol. Chem. *288*, 36149–36159. https://doi.org/10.1074/jbc.M113.507970.

32. DeLuca, K.F., Lens, S.M., and DeLuca, J.G. (2011). Temporal changes in Hec1 phosphorylation control kinetochore-microtubule attachment stability during mitosis. J. Cell Sci. *124*, 622–634. https://doi.org/10.1242/jcs.072629.

33. Foley, E.A., Maldonado, M., and Kapoor, T.M. (2011). Formation of stable attachments between kinetochores and microtubules depends on the B56-PP2A phosphatase. Nat. Cell Biol. *13*, 1265–1271. https://doi.org/10.1038/ncb2327.

34. Sarangapani, K.K., Koch, L.B., Nelson, C.R., Asbury, C.L., and Biggins, S. (2021). Kinetochore-bound Mps1 regulates kinetochore-microtubule attachments via Ndc80 phosphorylation. J. Cell Biol. *220*, e202106130. https://doi.org/10.1083/jcb.202106130.

35. Tighe, A., Johnson, V.L., and Taylor, S.S. (2004). Truncating APC mutations have dominant effects on proliferation, spindle checkpoint control, survival and chromosome stability. J. Cell Sci. *117*, 6339–6353. https://doi.org/10.1242/jcs.01556.

36. Natsume, T., Kiyomitsu, T., Saga, Y., and Kanemaki, M.T. (2016). Rapid protein depletion in human cells by auxin-inducible Degron tagging with short homology donors. Cell Rep. *15*, 210–218. https://doi.org/10.1016/j.celrep.2016.03.001.

37. Schindelin, J., Arganda-Carreras, I., Frise, E., Kaynig, V., Longair, M., Pietzsch, T., Preibisch, S., Rueden, C., Saalfeld, S., Schmid, B., et al. (2012). Fiji: an open-source platform for biological-image analysis. Nat. Methods *9*, 676–682. https://doi.org/10.1038/nmeth.2019.

38. R Core Team. (2015). RStudio: integrated development environment for R.

39. Wickham, H., Averick, M., Bryan, J., Chang, W., McGowan, L., François, R., Grolemund, G., Hayes, A., Henry, L., Hester, J., et al. (2019). Welcome to the Tidyverse. J. Open Source Software *4*, 1686. https://doi.org/10.21105/joss.01686.

40. Alfonso-Pérez, T., Hayward, D., Holder, J., Gruneberg, U., and Barr, F.A. (2019). MAD1-dependent recruitment of CDK1-CCNB1 to kinetochores promotes spindle checkpoint signaling. J. Cell Biol. *218*, 1108–1117. https://doi.org/10.1083/jcb.201808015.

41. Ridler, T.W., and Calvard, S. (1978). Picture thresholding using an iterative selection method. IEEE Trans. Syst. Man Cybern. *8*, 630–632. https://doi.org/10.1109/TSMC.1978.4310039.

STAR★METHODS

KEY RESOURCES TABLE

REAGENT or RESOURCE	SOURCE	IDENTIFIER
Antibodies		
Astrin Rabbit pAb	Thein et al.[17]	N/A
BUB1 Rabbit pAb	Bethyl	Cat#A300-373A; RRID: AB_2065943
BUBR1 Rabbit pAb	Bethyl	Cat#A33-386A; RRID: AB_386097
CENP-C Guinea Pig pAb	MBL	Cat#PD030; RRID: AB_10693556
CREST Human pAb	Antibodies	Cat#15-234-0001; RRID: AB_2687472
HEC1 Mouse mAb (9G3.23)	GeneTex	Cat#GTX70268; RRID: AB_371632
MAD1 Rabbit pAb	GeneTex	Cat#GTX105079; RRID: AB_11173437
MPS1 Mouse mAb (N1)	Abcam	Cat#ab11108; RRID: AB_297757
Myc Mouse mAb (pE10)	Sigma-Aldrich	Cat#M4439; RRID: AB_439694
p-Histone H3 Ser10 – pH3S10 Mouse mAb (6G3)	Cell Signaling	Cat#9706S; RRID: AB_331748
Phospho-Aurora Kinase B (Thr232) Rabbit pAb	ThermoFisher Scientific	Cat#600-401-677; RRID: AB_2061641
Tubulin Mouse mAb (DM1A)	Sigma-Aldrich	Cat#T6199; RRID: AB_477583
Tubulin Rabbit mAb (EP1332Y)	Abcam	Cat#ab52866; RRID: AB_869989
HURP Sheep pAb	Dunsch et al.[19]	N/A
KNL1 Sheep pAb	This paper	N/A
Beta Actin Mouse mAb (AC-15) HRP conjugate	Abcam	Cat#ab49900; RRID:AB_867494
Alexa Fluor 647 AffiniPure Donkey Anti-Guinea Pig IgG (H+L)	Stratech	Cat#706-605-148; RRID: AB_2340476
Donkey anti-Mouse IgG (H+L) Highly Cross-Adsorbed Secondary Antibody, Alexa Fluor 555	ThermoFisher Scientific	Cat#A31570; RRID: AB_2536180
Donkey anti-Sheep IgG (H+L) Cross-Adsorbed Secondary Antibody, Alexa Fluor 555	ThermoFisher Scientific	Cat#A21436; RRID: AB_2535857
Donkey anti-Rabbit IgG (H+L) Highly Cross-Adsorbed Secondary Antibody, Alexa Fluor 555	ThermoFisher Scientific	Cat#A31572; RRID: AB_162543
Donkey anti-Mouse IgG (H+L) Highly Cross-Adsorbed Secondary Antibody, Alexa Fluor 350	ThermoFisher Scientific	Cat#A10035; RRID: AB_2534011
Donkey anti-Rabbit IgG (H+L) Highly Cross-Adsorbed Secondary Antibody, Alexa Fluor 350	ThermoFisher Scientific	Cat#A10039; RRID: AB_2534015
Donkey anti-Rabbit IgG (H+L) Highly Cross-Adsorbed Secondary Antibody, Alexa Fluor 647	ThermoFisher Scientific	Cat#A31573; RRID: AB_2536183
Donkey anti-Mouse IgG (H+L) Highly Cross-Adsorbed Secondary Antibody, Alexa Fluor 647	ThermoFisher Scientific	Cat#A31571; RRID: AB_162542
Donkey anti-Human IgG (H+L) Secondary Antibody [DyLight 350]	Bio-Techne	Cat# NBP2-60667UV; RRID: AB_2556705
Peroxidase AffiniPure Donkey Anti-Rabbit IgG (H+L)	Stratech	Cat#711-035-152; RRID: AB_10015282
Peroxidase AffiniPure Donkey Anti-Mouse IgG (H+L)	Stratech	Cat#715-035-151; RRID: AB_2340771

(*Continued on next page*)

Continued

REAGENT or RESOURCE	SOURCE	IDENTIFIER
Chemicals, peptides, and recombinant proteins		
AZ3146 - used 2 μM	Tocris Bioscience	Cat#3994
ZM447439 – used at 10 μM	Tocris Bioscience	Cat#2458
Calyculin A – used at 25 nM	Tocris Bioscience	Cat#1336
S-trityl-L-cysteine – used at 10 μM	Sigma-Aldrich	Cat#164739-5G
Rapamycin – used at 500 nM	Sigma-Aldrich	Cat#R0395
MG132 – used at 20 μM	Santa Cruz Biotechnology	Cat#sc-201270
Doxycycline – used at 2μM	Insight	Cat#sc-204743
SiR-Tubulin – used at 50 nM	Spirochrome	Cat#SC002
SiR-DNA – used at 50 nM	Spirochrome	Cat#SC007
Nocodazole – used at 0.6 μM	Merck Chemicals	Cat#484728
Hoechst 33342 – used at 4 μM	ThermoFisher Scientific	Cat#H3570
Oligofectamine	ThermoFisher Scientific	Cat#12252011
TransIT-LT1	Mirus-Bio	Cat#MIR2300
Gibco DMEM, high glucose, GlutaMAX Supplement, pyruvate	ThermoFisher Scientific	Cat#31966047
Fluorobrite	ThermoFisher Scientific	Cat#A1896701
Glutamax supplement	ThermoFisher Scientific	Cat#35050061
TrypLE Express Enzyme	ThermoFisher Scientific	Cat#12605036
Blasticidin hydrochloride	Invivogen	Cat#ant-bl-1
Hygromycin B Gold	Invivogen	Cat#ant-hg-5
Puromycin	Invivogen	Cat#ant-pr
Experimental models: Cell lines		
HeLa S3	ATCC	Cat#CCL-2.2; RRID: CVCL_0058
HeLa S3 with MPS1 endogenously tagged with GFP at the C terminus	Hayward et al.[21]	N/A
HeLa S3 with MPS1 endogenously tagged with GFP at the C terminus with Aurora-B kinetochore targeting system (plasmid AAVS1CRISPR_inducible miRFKBP5_ Mis12-GFP-FKBP3:mCherry-FRB-INCENP 47-918) integrated at AAVS1 locus	This paper	N/A
HeLa S3 Flp-In-TRex parental cells	Tighe et al.[35]	N/A
HeLa S3 Flp-In-TREx GFP-MPS1 (WT)/(KD)/ (N8A)/(N8E)	This paper	N/A
HeLa S3 Flp-In-TREx B56 Delta	This paper	N/A
HeLa S3 Flp-In-TRex parental cells with MPS1 endogenously tagged with GFP at the N terminus	This paper	N/A
HeLa S3 Flp-In-TREx mCherry-BUBR1 (WT)/(LI/AA) - with MPS1 endogenously tagged with GFP at the N terminus	This paper	N/A
HeLa S3 Flp-In-TREx Hec1-mCherry (WT)/ (9A)/(9D) - with MPS1 endogenously tagged with GFP at the N terminus	This paper	N/A
Oligonucleotides		
Control siRNA against GL2 (luciferase) (5'-CGUACGCGGAAUACUUCGAUU-3')	Dharmacon	Cat#D-001100-01-20
siRNA against MPS1 3'UTR (5'-UUGGACUGUUAUACUCUUGAA-3', 5'-GUGGAUAGCAAGUAUAUUCUA-3', and 5'-CUUGAAUCCCUGUGGAAAU-3')	Hayward et al.[21]	N/A

(*Continued on next page*)

Continued

REAGENT or RESOURCE	SOURCE	IDENTIFIER
siRNA against HEC1 5'UTR (5'-CCCUGGGUCGUGUCAGGAA-3')	Nijenhuis et al.[12]	N/A
siRNA against BUBR1 3'UTR (5'-GCAATCAAGTCTCACAGAT-3')	Espert et al.[24]	N/A
On-target plus Smartpool siRNA oligos against PPP2R5A (5'-GCUCAAAGAUGCCACUUCA-3', 5'-CAAUACAAGUGCCGAAUAA-3', 5'-UGAAUGAACUGGUUGAGUA-3', 5'-GGAAAUGAAUGGCAAGCUU-3')	Dharmacon	Cat#L-009352
On-target plus Smartpool siRNA oligos against PPP2R5B (5'-CGCAUGAUCUCAGUGAAUA-3', 5'-UCAAGUCGCUGUCUGUCUU-3', 5'-CAAACCAUCGUAUCACUGA-3', 5'-GAACAAUGAGUAUAUCCUA-3')	Dharmacon	Cat#L-009366
On-target plus Smartpool siRNA oligos against PPP2R5C (5'-GGAUUUGCCUUACCACUAA-3', 5'-GGAAGAUGAACCAACGUUA-3', 5'-CAUCAGAAUUUGUGAAGAU-3', 5'-CAGAAGUAGUCCAUAUGUU-3')	Dharmacon	Cat#L-009433
On-target plus Smartpool siRNA oligos against PPP2R5D (5'-GUACAUCGACCAGAAGUUU-3', 5'-UCCAUGGACUGAUCUAUAA-3', 5'-UGACUGAGCCGGUAAUUGU-3', 5'-GUAGGCAGAUCAACCACAU-3')	Dharmacon	Cat#L-009799
On-target plus Smartpool siRNA oligos against PPP2R5E (5'-UUAAUGAACUGGUGGACUA-3', 5'-GCACAGCUGGCAUAUUGUA-3', 5'-GACACGCUAUCUGAUCUUA-3', 5'-GGAUAAAGUAGACGGAUUU-3')	Dharmacon	Cat#L-008531
Recombinant DNA		
Plasmid: MPS1 N-terminal GFP CRISPR	This paper	N/A
Plasmid: AAVS1CRISPR_inducible miRFKBP5_Mis12-GFP-FKBP3:mCherry-FRB-INCENP 47-918	This paper, adapted from plasmids pERB109 and pMK232 (Addgene #28280 and #72834) Ballister et al.[30]; Natsume et al.[36]	N/A
Plasmids: pcDNA5-mCherry-BUBR1 WT, LI/AA	Espert et al.[24]	N/A
Plasmids: pcDNA5-GFP-MPS1 WT, KD, N8A, N8E	This paper and Hayward et al.[10]	N/A
Plasmids: pcDNA5-HEC1-mCherry WT, 9A, 9D	This paper	N/A
Plasmid: pcDNA5-GFP-B56 Delta	This paper	N/A
Software and algorithms		
FIJI distribution of ImageJ v1.52q-v1.53s	NIH image; Schindelin et al.[37]	https://imagej.nih.gov/ij/; RRID: SCR_003070
R v4.0.0	R Core Team	http://www.r-project.org; RRID: SCR_001905
RStudio v1.3.959	RStudio Team[38]	http://www.rstudio.com; RRID: SCR_000432

(*Continued on next page*)

Continued

REAGENT or RESOURCE	SOURCE	IDENTIFIER
Tidyverse v1.3.0	Wickham et al.[39]	https://cran.r-project.org/package=tidyverse; RRID: SCR_019186
GraphPad PRISM v9.2.0	GraphPad Software	https://www.graphpad.com; RRID: SCR_002798
ImageJ Macros	This paper	Zenodo: https://doi.org/10.5281/zenodo.7215770

RESOURCE AVAILABILITY

Lead contact

Further information and requests for resources and reagents should be directed to and will be fulfilled by the lead contact, Dr Ulrike Gruneberg (ulrike.gruneberg@path.ox.ac.uk).

Materials availability

Plasmids and cell lines generated in this study are available on request.

Data and code availability

- All data reported in this paper will be shared by the lead contact upon request.
- All original ImageJ macros described in method details have been deposited at Zenodo and are publicly available as of the date of publication. DOIs are listed in the key resources table.
- Any additional information required to reanalyze the data reported in this paper is available from the lead contact upon request.

EXPERIMENTAL MODEL AND SUBJECT DETAILS

Cell lines

HeLa (Henrietta Lacks) cells were cultured in DMEM with 1x GlutaMAX (Life Technologies) containing 10% [vol/vol] bovine calf serum at 37°C and 5% CO2. HeLa cells homozygously expressing endogenously tagged MPS1-GFP[21] were selected with 550 μg/ml geneticin. HeLa Flp-In TREx cells[35] were maintained in DMEM with 1x GlutaMAX (Life Technologies) containing 10% [vol/vol] bovine calf serum and 4 μg/ml blasticidine and 200 μg/ml hygromycin B at 37°C and 5% CO2. HeLa Flp-In TREx cells expressing endogenously tagged GFP-MPS1 were maintained in medium additionally containing 0.2 μg/ml puromycin. HeLa cells expressing endogenously tagged MPS1-GFP as well as the rapamycin-dependent Aurora B kinetochore targeting system were grown in DMEM with 1x GlutaMAX (Life Technologies) containing 10% [vol/vol] bovine calf serum as well as 550 μg/ml geneticin and 1 μg/ml Puromycin.

Bacterial strains

For molecular biology, *E.coli* strain DH5α (Invitrogen, 18258-012) was used throughout the study. *E.coli* cells were cultured in standard LB medium supplemented with appropriate antibiotics at 37°C.

METHOD DETAILS

Molecular biology

Human MPS1, HEC1 and BUBR1 were amplified from Human testis cDNA (Marathon cDNA; Takara Bio) using Pfu polymerase (Promega). Mammalian expression constructs were made using pcDNA5/FRT/TO vectors (Invitrogen), modified to encode the EGFP- or mCherry-reading frames. BUBR1 mutagenesis has been described previously[24] as has generation of MPS1 kinase-dead mutants.[10] To generate phospho-null (N8A) or phospho-mimetic (N8E) MPS1 autophosphorylation sites, the first 300 base pairs of MPS1 were synthesized by Twist Bioscience with the sites encoding amino acids Ser7, Thr12, Ser15, Thr33, Ser37, Thr45, Thr46 and Ser49 changed to encode either alanine (N8A) or glutamic acid (N8E) residues. HiFi assembly (NEB) was then used to replace the first 300 base pairs of MPS1 with the synthetic fragments in expression vectors. The HEC1-9A and 9D mutants[32] were generated by gene synthesis and cloned into pcDNA5/FRT/TO encoding a C-terminal GFP-fusion.

Cell line generation

HeLa cells homozygously expressing MPS1 endogenously tagged with GFP at the C-terminus have been described before.[21] HeLa cell lines with single integrated copies of the desired transgene were created using the T-Rex doxycycline-inducible Flp-In system (Invitrogen[35]) using pcDNA5/FRT/TO vectors. MPS1 was endogenously tagged at the N-terminus with GFP using CRISPR/Cas9

editing in HeLa cells already containing a single T-Rex doxycycline-inducible Flp-In integration site using a previously described method.[21,40] In brief, homology recombination cassettes containing the desired knock-in DNA with flanking regions of homology of 1075 bp to the target locus were co-transfected with a version of pSpCAS9(BB) (Addgene, #48139) containing the guide RNA sequence 5'-TCTTTGATGCTAGTTAAAGT-3' and modified to remove puromycin resistance. The knock-in sequences harbor a puromycin resistance marker followed by a glycine-serine rich flexible linker (GS), a P2A ribosome-skipping sequence, and the EGFP protein sequence followed by a glycine-serine rich flexible linker (GS). Antibiotic-resistant clones were selected and successful modification was confirmed by western blotting.

INCENP kinetochore recruitment by rapamycin addition was achieved by editing a previously described system (plasmid pERB109, Addgene #58280).[30] This was adapted by placing miRFKBP5_Mis12-GFP-FKBP3 under doxycycline-inducible expression and replacing GFP with a Myc tag. INCENP 47-918 was inserted after mCh-FRB. 831 and 804 bp homology arms flanking the AAVS1 safe harbour locus were also added, and the system was stably integrated into the AAVS1 safe harbour locus of HeLa cells homozygously expressing MPS1 endogenously tagged with GFP at the C-terminus by CRISPR/Cas9 knock-in, using the guide RNA sequence 5'-GTTAATGTGGCTCTGGTTCT-3' (Addgene constructs #72833 and #72834[36]).

RNAi and RNAi rescue assays

All siRNA depletions were performed for 48 hours. Control siRNA was performed against GL2 (luciferase) (5'-CGUACGCGGAAUA CUUCGAUU-3') (Dharmacon (#D-001100-01-20). siRNA oligos targeting PP2A-B56 have been described previously[24] and were purchased from Dharmacon. All other siRNA oligonucleotides were purchased from ThermoFisher Scientific. RNAi rescues assays with GFP-MPS1/mCherry-BUBR1/mCherry-HEC1 transgenes were all performed using the same protocol in which siRNA depletion was carried out for 48 hours in total. Transgene induction was initiated with the addition of 2 μM doxycycline (InvivoGen) 2 hours prior to siRNA addition. Endogenous MPS1 was depleted using oligonucleotides against the 3' UTR (5′-UUGGACUGUUAUACUCUUGAA-3′, 5′-GUGGAUAGCAAGUAUAUUCUA-3′, and 5′-CUUGAAUCCCUGUGGAAAU-3′).[21] Endogenous HEC1 was depleted using oligonucleotides against the 5' UTR (5'-CCCUGGGUCGUGUCAGGAA-3').[12] Endogenous BUBR1 was depleted using oligonucleotides against the 3' UTR (5′-GCAATCAAGTCTCACAGAT-3′).[24] A second induction was performed 24 h into the siRNA depletion.

Drug and cold treatments

Nocodazole (0.6 μM) treatments of cells to depolymerize microtubules and arrest the cells in a prometaphase-like state were performed for 2 hours. STLC (10 μM) treatment to inhibit Eg5 kinesin and generate monopolar spindles was also performed for 2 hours. MG132 (20 μM) to inhibit the proteasome and arrest cells in metaphase was performed for 30 min. MPS1 inhibition was performed using AZ3146 (2 μM) for 15 min. Aurora B inhibition was performed using ZM447439 (10 μM) for 10 min. When cells arrested in nocodazole or STLC were treated with AZ3146 or ZM447439, or in experiments with the MPS1 phospho-mutants, the proteasome inhibitor MG132 (20 μM) was added 30 min prior to fixation to prevent premature mitotic exit. Rapamycin was added at 500 nM, with times indicated in figures. Mitotic cells were cold treated by placing cell dishes on ice and replacing the existing media with media (DMEM with 1% (vol/vol) GlutaMAX (Life Technologies) containing 10% (vol/vol) bovine calf serum) at 4°C. Cells remained on ice for 9 min then were fixed at room temperature.

Immunofluorescence staining

Cells were fixed with PTEMF buffer (20mM PIPES-KOH pH 6.8, 0.2% v/v Triton X-100, 10mM EDTA, 1mM $MgCl_2$, 4% v/v formaldehyde) for 12 minutes at room temperature. Coverslips were incubated in blocking buffer (3% w/v bovine serum albumin, 0.1% v/v Triton X-100 in PBS) for a minimum of 45 minutes. Coverslips were incubated face-down on 80μl droplets of primary antibodies in a humidified chamber for 1 hour. Following primary antibody incubation coverslips were washed 3 x in PBS. Secondary donkey antibodies against mouse, rabbit, guinea pig, or sheep, labelled with Alexa Fluor 405, Alexa Fluor 488, Alexa Fluor 555, or Alexa Fluor 647 (Molecular Probes) were used at 1:1000. Coverslips were incubated face-down on 80μl droplets of diluted antibodies in a humidified chamber for 45 minutes. Coverslips were washed 3 x in PBS and 1 x in distilled deionised water. Coverslips were left to dry completely before being mounted with 7μl of Mowiol 4-88 (Sigma) according to manufacturer's instructions. For the images in Figure 2G and for inter-kinetochore distance measurements, coverslips were mounted onto droplets of Vectashield Plus (2bscientific) and sealed with clear nail polish.

Immunofluorescence microscopy

Samples seeded on #1.5 thickness coverslips were imaged on a DeltaVision Core light microscopy system (GE Healthcare) using a 100×/1.4-NA objective fitted to an Olympus IX-71 microscope stand. Standard filter sets for DAPI (excitation 390/18, emission 435/48), FITC (excitation 475/28, emission 525/48), TRITC (excitation 542/27, emission 597/45), and Cy-5 (excitation 632/22, emission 676/34) were used to sequentially excite and collect fluorescence images on a CoolSnap HQ2 CCD camera (Photometrics) using the software package softWoRx (GE Healthcare). Cells were imaged using a 0.2-μm interval and a total stack of 2 μm and deconvolved for presentation using softWoRx. For quantification, imaging was performed using a 60×/1.35-NA oil-immersion objective on a BX61 Olympus microscope equipped with filter sets for DAPI, EGFP/Alexa Fluor 488, 555, and 647 (Chroma Technology), a CoolSNAP HQ2 camera (Roper Scientific), and MetaMorph 7.5 imaging software (GE Healthcare).

Super-resolution immunofluorescence microscopy

Samples seeded on #1.5 thickness coverslips were imaged on an Olympus SoRa spinning disk confocal microscope using a 60x/1.5-NA objective fitted to an Olympus IX-83 microscope stand with 3.2 x optical zoom and a Yokogawa CSU-W1 SoRa super-resolution spinning disk. Solid state lasers emitting 405 nm, 488 nm, 561 nm and 633 nm were used. Images were captured with a Prime BSI sCMOS camera (photometrics) using Olympus cellSens software package. Images were acquired with a 0.24 μm interval over a total distance of 4.8 μm. Constrained iterative deconvolution was performed on cellSens.

Live cell imaging

Cells seeded on circular glass bottom Fluorodish imaging dishes (World Precision Instruments) in Fluorobrite media (ThermoFisher Scientific) supplemented with 10% [vol/vol] FBS and 1x GlutaMAX (ThermoFisher Scientific) were imaged at 37°C with 5% CO_2 on an Olympus SoRa spinning disk confocal microscope using a 60x/1.5-NA or 100x/1.45-NA objective fitted to an Olympus IX-83 microscope stand with a Yokogawa CSU-W1 SoRa super-resolution spinning disk. Solid state lasers emitting 405 nm, 488 nm, 561 nm and 633 nm were used. Images were captured with a Prime 95B sCMOS camera (photometrics) using Olympus cellSens software package. Kinetochores of STLC arrested cells were imaged using the 100x/1.45-NA objective as 1.3 μm stacks with intervals of 0.26 μm across a period of 15 minutes with 30 second intervals. STLC (10 μM) was added 4 hours prior to imaging. 10 μm stacks with intervals of 0.5 μm of MG132/Nocodazole arrested cells were imaged using the 60x/1.5-NA objective at intervals of 2 min over a total period of 22 minutes, with 100 ul PBS + Rapamycin added in the interval between the first a second timepoint. SiR-Tubulin (50 nM) and Hoechst (4 μM) were added 1 hour prior to imaging.

For determining mitotic timings of GFP-MPS1 Flp-In TREx cell lines, cells were seeded on 6-well #1.5H glass-bottomed dishes (Cellvis) in Fluorobrite media (ThermoFisher Scientific) supplemented with 10% [vol/vol] FBS and 1x GlutaMAX (ThermoFisher Scientific). Imaging was performed using a 20x/0.75 NA air objective on an EVOS M7000 (ThermoFisher) with software version 2.0.2094.0, equipped with an onstage incubator and DAPI, GFP, Texas Red, and Cy5 light cubes. Cells were imaged at 37°C under 5% CO2 every 5 minutes for 12 hours. At each time point and stage position a stack of 4 z-planes was taken spaced 3μm apart were acquired. SiR-DNA was added 1 hour prior to imaging.

For FRAP measurements of GFP-MPS1 Flp-In TREx cell lines, cells were seeded on 35mm Fluorodish imaging dishes (World Precision Instruments) in Fluorobrite media (ThermoFisher Scientific) supplemented with 10% FBS and 1x GlutaMAX (ThermoFisher Scientific). Imaging was performed using an IX81 (Olympus) coupled to an Ultraview Vox spinning disk confocal system (PerkinElmer) fitted with an EM-CCD camera (C9100-13; Hamamatsu Photonics) and on-stage incubator (Tokai Hit), using a 60×/1.42 NA oil immersion objective. Cells were imaged at 37°C under 5% CO_2. Nocodazole was added to cells 1 hour prior to imaging. A 488nm (GFP) laser was used to image a single focal plane every 250ms for 1 second prior to the bleach step. Following this, the 488nm laser was used to perform a 1 second bleach step at 100% power over a single kinetochore. Subsequently, images of the same focal plane were taken every 250ms for 60 seconds using the 488nm laser.

QUANTIFICATION AND STATISTICAL ANALYSIS

Image processing and analysis

Image processing and analysis was performed using the Fiji distribution of ImageJ.[37] For figures, deconvolved images acquired on a DeltaVision Core light microscopy system were cropped to 350 x 350px and maximum projected. Channels were subject to linear contrast adjustment. Within each figure contrast adjustment of each channel is the same between conditions and merges.

Quantitation was performed on images of cells from a BX61 Olympus microscope which were cropped to 250 x 250px and sum projected through 7 z-slices. Kinetochore intensities for each fluorescence channel were determined by placing 8px-diameter circular ROIs at the maxima of individual non-overlapping kinetochores and measuring the mean pixel intensity of each channel within said selections. Where possible 20 kinetochores were measured per cell. Background measurements were derived by taking an equivalent number of pixels as were in the ROI which were as close as possible to the ROI without overlapping with kinetochores. In brief, a binary mask of kinetochore signal was generated by performing a tophat transform of the CENP-C channel and thresholding using an iterative intermeans method.[41] Pixels were radially selected from outside the kinetochore ROI and, if not overlapping with signal in the binary kinetochore mask, added to a new background ROI. Once 52px had been incorporated into the background ROI the mean pixel intensity of each channel within said ROI was measured.

Data analysis was performed in Rstudio[38] using the Tidyverse collection of packages.[39] Kinetochore signal intensities were background-adjusted by subtracting the background signal on a channel-by-channel basis. Next, the mean intensity of the channel of interest was divided the mean intensity of the CENP-C channel on a per-kinetochore basis. The mean kinetochore localization intensities were then calculated for each cell. Normalization was performed within repeats by dividing each cell's mean kinetochore localization intensity by that of the group which was being normalized to.

Measurements of microtubule width, and of HURP and Tubulin intensity on attached K-fibers, were performed in Fiji on DeltaVision acquired images prior to deconvolution. Microtubule width was measured on single Z-planes of metaphase microtubule bundles which were clearly attached to a kinetochore and had no adjacent microtubule bundles. A 1 μm line was drawn from the center of the kinetochore through the axis of the microtubule, then the line was rotated 90° so that the line was perpendicular to the microtubule and 0.5 μm away from the kinetochore. Measurements of pixel intensity along the line were taken. A subsequent 1 μm line was then drawn parallel to the microtubule bundle and the average pixel intensity along that line was subtracted as background signal.

Measurements of HURP and Tubulin intensity were taken from projected images stack of STLC or MG132 arrested cells respectively. Measurements were only taken from microtubule bundles which were clearly attached to a kinetochore and had no adjacent microtubule bundles. Measurements were recorded from a circular ROI with a 0.25 μm radius placed 0.5 μm (Tubulin) or 2 μm (HURP) from the edge of the kinetochore at the center of the microtubule bundles. An adjacent cytoplasmic circular ROI was also measured and that value subtracted as background. Inter-kinetochore distances were determined by measuring the x, y and z coordinates of the maxima of anti-KNL1 kinetochore staining at sister kinetochores pairs. Kinetochore pairs were ascertained based on CREST staining of the centromeric region between the sister kinetochores.

In cells expressing the Aurora B kinetochore targeting system, measurements of anti-AurB-pT232 following mCherry-FRB-INCENP recruitment to kinetochores were performed by measuring the mean intensity of anti-AurB-pT232 and CREST staining within a 4-pixel radius ROI centred around kinetochores as determined by the CREST staining. This ROI encompassed kinetochores and centromeres at unattached kinetochores (Nocodazole), but only kinetochores at metaphase kinetochores (MG132). A measurement of adjacent chromatin Aurora B pT232 and CREST staining were taken as background measurements and subtracted from the kinetochore/centromere values. AurB-pT232 values were subsequently divided by the CREST values for normalisation. 20 kinetochores were measured per cell. Measurements were normalised to the Nocodazole treated condition.

Sister chromatid cohesion following mCherry-FRB-INCENP recruitment to aligned kinetochores in cells expressing the Aurora B kinetochore targeting system was measured by counting the proportion of joined kinetochore pairs. Joined kinetochores demonstrate a ''bridge'' of CREST staining the centromeric region between the individual kinetochores, as marked by CENP-C staining. When sister chromatid cohesion is lost, there is no longer a CREST bridge joining the two kinetochores. As a control, loss of sister chromatid cohesion was induced by the addition of 2 μM of MPS1 inhibitor AZ3146 for 20 minutes in the absence of MG132.

The cold stability of mitotic spindles in cells expressing the Aurora_B kinetochore targeting system, and in cells depleted of PP2A-B56, was measured by classifying mitotic spindles as either: having no spindle (majority of kinetochores clearly not attached to microtubules), having a disorganised spindle (majority of kinetochores attached to microtubules but not aligned at a metaphase, or having an organised bipolar spindle (majority of kinetochores attached to microtubules and aligned at the metaphase plate).

Anti-Histone H3 pSer10 (H3pS10) staining on chromatin was measured by creating a binary mask of chromatin based on Hoechst staining. The area of this mask and total fluorescence signal of anti-H3pS10 was measured, as was the average anti-H3pS10 fluorescence in an adjacent area of cytoplasm. The average cytoplasmic background signal was multiplied by the area of the chromatin binary mask and subtracted from the total chromatin anti-H3pS10 signal. Measurements were normalised to the mean fluorescence of the control condition.

Analysis of kinetochore MPS1-GFP and mCherry-FRB-INCENP-47-918 from live imaging was performed by placing five 8 pixel-diameter circular ROIs over MPS1 positive kinetochores at the first timepoint they were visible. The same ROIs were then measured at previous timepoints. ROIs were moved where needed at subsequent timepoint to track the same kinetochores. Background measurements were taken from 5 chromatin free cytoplasmic regions. Where no MPS1 positive kinetochores were visible, ROIs were taken from 5 points of the mitotic plate, as defined by Hoechst staining. Chromosome misalignment was measured by generating a rectangular ROI at timepoint 0 which covered the metaphase plate as defined by Hoechst staining, and measuring the intensity of Hoechst staining. A second measurement was taken of the total level of Hoechst staining in the cell (the cell boundary defined by cytoplasmic GFP signal). A third measurement was made of the average background intensity outside of the cell, which was multiplied by the area of either the metaphase plate ROI or whole cell ROI, and subtracted from those values. A percentage of chromatin outside of the metaphase plate could then be ascertained and reported as percent of chromosomes that are misaligned. This was performed for each timepoint, with the rectangular ROI measuring the area of the metaphase plate moved where needed to be covering what remained of the metaphase plate and so as to be perpendicular with the spindle axis, as defined by SiR-Tubulin staining. Where chromosome misalignment was severe and SiR-Tubulin staining demonstrated that no microtubules remained in the vicinity of the area previously occupied by the metaphase plate, the level of chromosome misalignment was set as 100%.

Analysis of GFP-MPS1 mitotic timings on live cell data was performed on maximum projections of movies. DNA morphology was used to record at which timepoints cells entered NEBD or anaphase.

Analysis of GFP-MPS1 FRAP measurements was performed using an in-house ImageJ macro. Movies in which the kinetochores drifted out of the focal plane at any point were discarded. At each timepoint, following background correction, the signal from the bleached ROI was divided by that of the whole cell to correct for general photobleaching. This metric was then normalised to the average of that from the 4 pre-bleach timepoints. A single exponential fit was used to determine $t_{1/2}$ timings.

Statistical Analysis

All statistical analysis was performed using GraphPad Prism version 9.2.0 for Windows (GraphPad Software, San Diego, California USA, www.graphpad.com). Each cell measured was considered as a biological replicate (n), hence mean measurements calculated for each cell were used for statistical analysis. At least three independent repeats of each experiment were performed, with statistical analysis performed using a sum of biological replicates from all independent experiments. The precise n numbers (where n is the number of cells analysed) is indicated in the figures.

Data sets were tested for normal distribution via a D'Agostino-Pearson omnibus K2 test. If all groups in an experiment were normally distributed, then the means were compared using a parametric statistical test as follows. If only two groups were compared then an unpaired 2 tailed t-test was used (with Welch's correction if the groups had unequal standard deviations). If more than two groups were compared with equal standard deviations a one-way ANOVA was used, which if rejected was followed by a

Tuckey's multiple comparisons test. If more than two groups were compared with unequal standard deviations a Brown-Forsythe ANOVA was used, which if rejected was followed by a Dunn's multiple comparisons test.

If all groups did not exhibit a normal distribution then medians were compared using a non-parametric statistical test as follows. If only two groups were compared then a Mann-Whitney test was used. If more than two groups were compared then a Kruskal-Wallis test was used, which if rejected was followed by a Dunn's multiple comparisons test. Graphs display the mean± SEM. p-values are shown on graphs as follows: $p > 0.05$ = not significant (n.s.), $p \leq 0.05$ = *, $p \leq 0.01$ = **, $p \leq 0.001$ = ***, $p \leq 0.0001$ = ****.